Influence of binding affinity and blood plasma level on cerebral pharmacokinetics

and PET imaging characteristics of two novel xanthine PET radioligands for the A₁

adenosine receptor

Daniela Schneider^{1*}, Angela Oskamp¹, Marcus Holschbach², Bernd Neumaier², Dirk Bier², Andreas

Bauer 1,3

¹Institute of Neuroscience and Medicine - Molecular Organization of the Brain (INM-2),

Forschungszentrum Jülich GmbH, 52428 Jülich, Germany

²Institute of Neuroscience and Medicine - Nuclear Chemistry (INM-5), Forschungszentrum Jülich

GmbH, 52428 Jülich, Germany

³ Neurological Department, Medical Faculty, Heinrich-Heine-University, Universitätsstraße 1, 40225

Düsseldorf, Germany

*Correspondence: d.schneider@fz-juelich.de; Tel.: +49 2461 61-6330

Abbrev. Title: Imaging characteristics of new A₁AR tracers

Keywords: radiotracer, radioligand, A₁ adenosine receptor, positron emission tomography,

[18F]CPFPX, preclinical evaluation

1

Abstract

Introduction. The suitability of novel positron emission tomography (PET) radioligands for quantitative *in vivo* imaging is affected by various physicochemical and pharmacological parameters. In this study, the combined effect of binding affinity, lipophilicity, protein binding and blood plasma level on cerebral pharmacokinetics and PET imaging characteristics of three xanthine-derived A_1 adenosine receptor (A_1AR) radioligands was investigated in rats.

Methods. A comparative evaluation of two novel cyclobutyl-substituted xanthine derivatives, 8-cyclobutyl-3-(3-[18 F]fluoropropyl)-1-propylxanthine ([18 F]CBX) and 3-(3-[18 F]fluoropropyl)-8-(1-methylcyclobutyl)-1-propylxanthine ([18 F]MCBX), with the reference A₁AR radioligand 8-cyclopentyl-3-(3-[18 F]fluoropropyl)-1-propylxanthine ([18 F]CPFPX) was conducted. This evaluation included *in vitro* competition binding assays, *in vitro* autoradiography and *in vivo* PET imaging. Differences in cerebral pharmacokinetics and minimal scan duration required for quantification of cerebral distribution volume (V_T) were assessed.

Results. Measured K_i values of non-labeled CBX, MCBX and CPFPX were 10.0 ± 0.52 nM, 3.3 ± 0.30 nM and 1.4 ± 0.15 nM, respectively (n=3-4). *In vitro* autoradiographic binding patterns in rat brain were comparable between the radioligands, as well as the fraction of non-specific binding (1.0-1.9%). *In vivo* cerebral pharmacokinetics of the novel cyclobutyl-substituted xanthines differed considerably from that of [18 F]CPFPX. Brain uptake and V_T of [18 F]CBX were substantially lower despite the higher concentration of radiotracer in plasma. [18 F]MCBX showed comparable uptake and V_T , but faster cerebral kinetics than [18 F]CPFPX. However, the faster kinetics of [18 F]MCBX did not enable the quantification of cerebral V_T in a shorter scan time.

Conclusions. The combined effect of individual physicochemical and pharmacological properties of a radiotracer on its PET imaging characteristics cannot be readily predicted. *In vivo* performance of the xanthine A₁AR radioligands was mainly influenced by binding affinity; plasma concentrations and cerebral kinetics were of secondary importance.

Introduction

The investigation of molecular cerebral targets via positron emission tomography (PET) critically depends on the availability of suitable PET radiotracers. Since important imaging characteristics such as brain uptake, target-to-background ratio and minimal scan duration required for target quantification depend on the physicochemical and pharmacological characteristics of the radiotracer, precise adjustment of these properties is crucial in order to develop imaging agents which can be successfully applied *in vivo*. For example, high binding affinity is essential for an adequate signal-to-background ratio, but often also increases the scan duration required for quantification of receptor parameters. Moreover, high affinity may lead to non-negligible levels of receptor occupancy especially for sparse receptors, which hampers quantitative analyses and might also result in undesirable pharmacological effects [1].

The four currently known adenosine receptors (A₁, A_{2A}, A_{2B}, A₃) represent valuable targets for *in vivo* molecular imaging as their expression and regulation is associated with numerous physiological functions (e.g., regulation of sleep and arousal [2–4] and synaptic plasticity [5]) and pathophysiological conditions (e.g., Alzheimer's disease [6, 7], Parkinson's disease [8, 9], schizophrenia [10] and epilepsy [11]). In particular, the A₁ adenosine receptor (A₁AR) received significant scientific interest due to its high and ubiquitous, although not homogenous, expression in the brain. Several classes of A₁AR PET radiotracers have been developed to date [12, 13], including the xanthine-based A₁AR antagonists which were derived from the naturally occurring stimulant caffeine. Currently, the ¹⁸F-labeled xanthine derivative 8-cyclopentyl-3-(3-[¹⁸F]fluoropropyl)-1-propylxanthine ([¹⁸F]CPFPX, Fig. 1) is considered the gold standard for A₁AR imaging with PET [14, 15]. Numerous preclinical and clinical imaging studies have been successfully conducted with [¹⁸F]CPFPX [16–18]. However, continuous efforts have been made to develop [¹⁸F]CPFPX analogs that allow for further improvement of A₁AR PET imaging, especially in brain regions with low receptor abundance. The synthesis of analogs with higher metabolic stability has been a major focus of the development strategy [19], as [¹⁸F]CPFPX undergoes rapid hepatic metabolism in humans and

animals leading to a fast decline of the radiotracer blood plasma levels in vivo [20, 21]. Since radiotracer delivery to the brain is a critical parameter governing brain exposure, increasing the blood radiotracer concentration could also result in elevated levels of radiotracer in the brain. Variation of the xanthine C8 substituent, which was identified as a metabolic soft spot, led to analogous compounds with promising in vitro metabolic characteristics. In vivo blood pharmacokinetics of two cyclobutyl-substituted analogs, namely 8-cyclobutyl-3-(3-[18F]fluoropropyl)-([¹⁸F]CBX, Fig. and 3-(3-[18F]fluoropropyl)-8-(1-methylcyclobutyl)-1-1-propylxanthine 1) propylxanthine ([18F]MCBX, Fig. 1) have already been evaluated in rats [22]. [18F]CBX exhibited substantially higher plasma levels than [18F]CPFPX (twice as high), whereas [18F]MCBX showed comparable plasma levels, but considerably faster pharmacokinetics. Since the structural modifications also led to alterations in other important properties such as lipophilicity and protein binding, the cerebral imaging characteristics of the novel A₁AR radioligands cannot be predicted with certainty.

In the present study, brain pharmacokinetics of [¹⁸F]CBX and [¹⁸F]MCBX were evaluated in rats and compared to the current reference tracer [¹⁸F]CPFPX. Based on the results of *in vitro* binding experiments, autoradiography and *in vivo* PET imaging studies, the combined effect of individual physicochemical and pharmacological properties such as binding affinity and blood plasma levels on cerebral pharmacokinetics and overall imaging performance of the two candidate A₁AR radioligands was assessed.

Figure 1 about here

Methods

Chemicals

All reagents, solvents and buffer substances were purchased from Sigma-Aldrich (Steinheim, Germany) or Merck (Darmstadt, Germany). Isoflurane for anaesthesia was obtained from CP-Pharma (Burgdorf, Germany).

8-Cyclopentyl-3-(3-fluoropropyl)-1-propylxanthine (CPFPX), 8-cyclobutyl-3-(3-fluoropropyl)-1-propylxanthine (CBX), 3-(3-fluoropropyl)-8-(1-methylcyclobutyl)-1-propylxanthine (MCBX), 8-cyclobutyl-3-(3-mesyloxypropyl)-7-pivaloyloxymethyl-1-propylxanthine (CBX precursor) and 3-(3-mesyloxypropyl)-8-(1-methylcyclobutyl)-7-pivaloyloxymethyl-1-propylxanthine (MCBX precursor) were synthesized and characterized in-house as previously described [14, 23]. 8-Cyclopentyl-3-(3-tosyloxypropyl)-7-pivaloyloxymethyl-1-propylxanthine (CPFPX precursor) was purchased from ABX GmbH (Radeberg, Germany). Tritiated DPCPX ([³H]DPCPX) was purchased from American Radiolabeled Chemicals (St. Louis, MO, USA). Radiosynthesis of [¹8F]CPFPX, [¹8F]CBX and [¹8F]MCBX was accomplished as described in [22]. Radiochemical purity of all batches used for PET imaging was > 95%. Mean molar activity was 177 ± 98 GBq/μmol.

Animal experiments

Brain PET data were acquired in the framework of an extensive preclinical evaluation study aimed at comparing the *in vivo* plasma pharmacokinetics of [¹⁸F]CBX, [¹⁸F]MCBX and [¹⁸F]CPFPX in male Sprague Dawley rats [22]. All experiments were conducted in accordance with the German Animal Welfare Act and approved by governmental authorities (AZ 84-02.04.2014.A496).

In vitro binding studies

Brain membranes for A_1AR assays were prepared as described in [24]. In brief, frontal cortices from rat brains were homogenized for 1 min in 10 volumes of ice-cold 320 mM sucrose, by means of a Potter at 20000 rpm under external ice cooling. The homogenate was centrifuged at 1000 g for 10 min at 4°C. The pellet was discarded and the supernatant was centrifuged at 10000 g for 40 min at 4°C. The resulting pellet was washed once with buffer (50 mM Tris, pH 7.4) and resuspended in 10 volumes of buffer (same volume as for sucrose, see above), thereafter stored in aliquots (2000 μ L) at

-80°C. Protein estimation used a naphthol blue black photometric assay [25] after solubilization in 15% NH₄OH containing 2% sodium dodecyl sulfate (w/v); human serum albumin served as standard. Dissociation constant (K_d) of [3 H]DPCPX (2.07 \pm 0.34 nM) and inhibition constants (K_i) of CPFPX, MCBX and CBX for the A₁AR were obtained in competition experiments using [3 H]DPCPX as radioligand (0.32 \pm 0.01 nM). The assays were performed in triplicate by incubating membrane homogenates with a protein content of 17 µg immobilized in a gel matrix with the radioligand in a total volume of 1500 µl 50 mM Tris buffer (pH 7.4, 22°C). After an incubation time of 70 minutes, the immobilized membrane homogenates were washed with water for one minute and transferred into scintillation cocktail (5 ml each, Ultima Gold, Perkin Elmer). The radioactivity of the samples (bound radioactivity) was measured with a liquid scintillation counter (Beckman, USA). All binding data were calculated by non-linear curve fitting with a computer aided curve-fitting program (Prism version 4.0, GraphPad Software, Inc., La Jolla, USA).

In vitro autoradiographic studies

Whole brains of decapitated rats were rapidly dissected and immediately frozen in isopentane (-50°C). Sagittal brain slices (20 μm) were cut on a Leica CM3050 cryostat (Leica Biosystems, Nussloch, Germany) which was set to a temperature of -20°C. Brain slices were thaw-mounted onto silica-coated object slides, dried for 1 h at 37°C and stored in vacuum-sealed plastic bags at -80°C until use. For autoradiography, the slices were preincubated in 50 mM Tris buffer (pH 7.4, 21°C) for 10 min and subsequently incubated in 50 mM Tris buffer (pH 7.4, 21°C) containing 100 μM guanosine-5'-triphosphate (GTP) and 0.4-0.5 nM [¹⁸F]CBX, [¹⁸F]MCBX or [¹⁸F]CPFPX for 120 min. For estimation of non-specific binding, the competing ligand DPCPX (13 μM) was added to some incubations. The slices were washed twice in Tris buffer (21°C) for 1 min, immersed in deionized water (4°C) to remove salt and dried under a stream of dry, warm (30°C) air for about 15 min. Subsequently, the dry slices were exposed to a phosphor imaging plate for 3-5 min, scanned with a phosphor imager (BAS 5000, Fujifilm, Düsseldorf, Germany) and analyzed with appropriate software

(AIDA Image Analyzer V4.13, Raytest, Straubenhardt, Germany). To estimate total and non-specific binding of the radiotracers, regions of interest (ROIs) were drawn around the entire brain slices and deposited energies within these ROIs were quantified. Specific binding was calculated as the difference between total and non-specific binding. Mean values were determined from 7-8 incubated slices per radiotracer.

PET imaging

Adult male Sprague Dawley rats (4 animals per radiotracer) received a 180-min PET scan under isoflurane anesthesia on a Siemens Inveon PET/CT Multimodality System (Siemens, Erlangen, Germany). Injected radioactivity, amount and mass of radiotracer are given in Table 1. Prior to radiotracer administration, a 20-min transmission scan (57Co source) was carried out to correct for attenuation. PET acquisition started simultaneously with radiotracer injection. List-mode PET data were reframed into a dynamic sequence of 12x10 s, 6x30 s, 15x60 s, 8x300 s and 12x600 s frames. The data were corrected for random coincidences, scattered radiation and attenuation, rebinned into 2-dimensional sinograms (Fourier Rebinning Algorithm) and reconstructed via filtered backprojection (ramp filter, cutoff: 0.5). The final datasets consisted of 159 slices with an image voxel size (x, y, z) of 0.7764, 0.7764, 0.796 mm (matrix size (x, y, z, t): 128, 128, 159, 53). Input functions were created from metabolite-corrected blood plasma data. Blood and metabolite analyses were carried out according to the methods described in [22]. Briefly, blood samples (ca. 200 µl) were drawn from the femoral artery of catheterized rats at regular time intervals during the 180-min scan. The total blood sampling volume was kept below 10% of the circulating blood volume of the animal. Radioactivity concentration in whole blood and plasma were determined. Fractions of unchanged radiotracer and radiolabeled metabolites in plasma were assessed by radio-thin layer chromatography (TLC) analysis. Aliquots of plasma were mixed with 3 volumes of methanol/acetonitrile (50:50, v/v), and centrifuged for 5 min at 20,000 rcf to sediment precipitated protein. Aliquots (5 µL) of the supernatants were spotted on a TLC plate (SIL G-25), developed with ethyl acetate/hexane, (75:25, v/v), dried and subsequently imaged for 50 min with an InstantImager autoradiography system.

Table 1 about here

PET data analysis

Brain PET data were analyzed using the PMOD V 3.4 software package (PMOD Technologies LLC, Zürich, Switzerland). Three-dimensional regions of interest were drawn either manually or semiautomatically (iso-contour algorithm) around the entire brain. Whole brain time-activity curves (TACs) and standardized uptake values (SUVs) were calculated, assuming a specific density of 1 g/ml for brain tissue. Time-weighted average SUV images (time window: 0-60 min post injection (p.i.); SUV maximum set to 5 g/ml) were generated for visual illustration. Cerebral pharmacokinetics of [18F]CPFPX, [18F]MCBX and [18F]CBX were evaluated using both graphical and compartmental analyses. Metabolite corrected arterial plasma TACs served as input functions for kinetic modeling. Logan graphical analysis was used to determine total cerebral distribution volume (V_T) of the radiotracers. Individual transfer rate constants and macro parameters were estimated from compartment model fits of dynamic whole brain PET data. A two-tissue compartment model (2TCM) was applied to [18F]CPFPX and [18F]MCBX data, whereas for [18F]CBX, a one-tissue compartment model (1TCM) was used. Iterative fitting was performed using a Levenberg-Marquardt algorithm (non-linear least squares minimization procedure). Residual weighting took into account frame duration, radioactive decay and, if appropriate, measured uptake. The fractional blood volume was fixed to a value of 3.6% [26]. No correction was applied for the time delay between the blood and tissue activity curves. The impact of scan time on the constancy of V_T estimations was evaluated by remodeling shortened data sets which were generated by iteratively omitting the last time frame. A deviation of less than 5% between the V_T calculated from the full 180-min data set and the shortened data set was used as criterion for time independence.

Statistics

Values are given as mean (standard deviation, SD) unless stated otherwise. For statistical analyses, OriginPro 2015G (OriginLab, Northampton, USA) and GraphPad Prism 4 (GraphPad Software, La Jolla, USA) were used. Significant differences between the means of individual test groups were assessed by using an independent t-test or a one-way analysis of variance (one-way ANOVA) followed by a post-hoc Tukey test. The significance level was set to 0.05.

Results

Binding affinity in vitro

The K_i values of the test compounds at 22°C are listed in Table 2. Differences in K_i between the ligands were statistically significant (P < 0.05, one-way ANOVA with post hoc Tukey test). CPFPX bound to rat A_1AR with 3 times greater affinity than MCBX and 7 times greater affinity than CBX; resulting in the following rank order of binding affinity: CPFPX>MCBX>CBX.

Table 2 about here

In vitro autoradiography

In vitro autoradiographs of sagittal rat brain slices incubated with [18 F]CBX, [18 F]MCBX and [18 F]CPFPX are presented in Fig. 2. Comparable binding patterns were obtained with all three radiotracers. Highest accumulation of radioactivity was observed in hippocampus, thalamus, cerebellar cortex and neocortex, lowest values were found in bulbus olfactorius, midbrain and brain stem, which is consistent with the well established distribution of A_1AR in the rat brain [27, 28]. The fraction of non-specific binding of [18 F]CBX, [18 F]MCBX and [18 F]CPFPX in rat brain amounted to 1.7 \pm 0.25%, 1.9 \pm 0.24% and 1.0 \pm 0.09%, respectively.

Figure 2 about here

Brain PET images

Injected radioactivity, amount and mass of substance did not significantly differ between radiotracers (p > 0.05, one-way ANOVA, Table 1). PET images acquired after administration of $[^{18}F]CBX$, $[^{18}F]MCBX$ and $[^{18}F]CPFPX$ are shown in Fig. 3. Using $[^{18}F]CPFPX$ and $[^{18}F]MCBX$, the rat brain was clearly visualized. High accumulation of radioactivity was observed in A₁AR-rich structures such as thalamus, hippocampus, neocortex and cerebellum. In contrast, cerebral accumulation of $[^{18}F]CBX$ was very low. Only thalamus, hippocampus, cerebellum and neocortex showed noticeable accumulation of radioactivity, whereas brain regions with lower receptor density were not detectable.

Figure 3 about here

In vivo cerebral pharmacokinetics

Kinetics of [¹⁸F]CBX, [¹⁸F]MCBX and [¹⁸F]CPFPX in rat brain and plasma are compared in Fig. 4. Despite the higher concentration of radiotracer in plasma, cerebral uptake of [¹⁸F]CBX was considerably lower than that of [¹⁸F]CPFPX and [¹⁸F]MCBX. The brain SUV curve of [¹⁸F]CBX remained below the plasma SUV curve during the entire measurement period, indicating cerebral efflux of radiotracer rather than accumulation. Cerebral kinetics of [¹⁸F]MCBX deviated noticeably from that of [¹⁸F]CPFPX. Whole brain SUV curves of [¹⁸F]MCBX peaked earlier (at about 4 min) than SUV curves of [¹⁸F]CPFPX (at about 12 min) and dropped more steeply. However, peak SUV values were comparable for both tracers (about 4 g/ml).

Figure 4 about here

Graphical and compartmental analysis of brain PET data

Kinetic parameters describing cerebral radiotracer uptake and distribution were determined either graphically (Logan plot) or via compartmental modeling (Fig. 5). A 2TCM could be readily fitted to whole brain TACs of both [¹⁸F]MCBX and [¹⁸F]CPFPX. For these radiotracers, the application of a 2TCM was clearly superior to a 1TCM, as proved by lower Akaike information criterion values. In the case of [¹⁸F]CBX, the low accumulation of radiotracer in the brain and the resulting unfavorable

signal-to-background ratio hampered fitting of the four rate constants describing radiotracer transfer in the 2TCM. Accordingly, 1TCM fits were used to characterize cerebral pharmacokinetics of [18 F]CBX. Results of compartmental modeling and graphical analysis are given in Table 3. The minimal scan time for [18 F]CPFPX to reach time independence in estimation of cerebral V_T was 76 ± 20 min. With [18 F]MCBX, data sets of two animals could be truncated to 10 and 28 min, respectively, while fulfilling the criterion for time independence. With the other two measurements, the frequent lack of fit convergence impeded a reliable derivation of V_T from the shortened data sets. Consequently, these two data sets were truncated to 135 and 145 min, respectively.

Total distribution volumes were determined via Logan graphical analysis and compartmental modeling. V_T of [^{18}F]MCBX and [^{18}F]CPFPX were nearly identical, whereas V_T of [^{18}F]CBX was about 4 times lower. V_T values acquired via compartmental modeling corresponded closely to the values obtained graphically. Differences in specific distribution volume (V_S) between [^{18}F]MCBX and [^{18}F]CPFPX did not reach statistical significance. Values of K_1 and k_2 were significantly higher for [^{18}F]MCBX than for [^{18}F]CPFPX, whereas K_1/k_2 ratios were similar.

Figure 5 about here

Table 3 about here

Discussion

The development of suitable PET radiotracers for molecular imaging of the brain is still an ambitious task due to the numerous factors affecting the success of a candidate radiotracer. Although the effect of individual physicochemical and pharmacological properties on the *in vivo* performance of a radiotracer is relatively well established, the mutual interactions between these factors and their overall impact on PET imaging are not sufficiently understood.

In this study, the effect of simultaneous alterations in radiotracer binding affinity, lipophilicity, protein binding and plasma pharmacokinetics on PET image quality was investigated using three

xanthine-derived radioligands developed for A_1AR imaging. The two novel cyclobutyl-substituted analogs of the reference radiotracer [^{18}F]CPFPX have been developed with the objective to improve A_1AR imaging by optimization of radiotracer metabolic stability.

In vitro binding experiments revealed that the replacement of the cyclopentyl moiety of CPFPX by a cyclobutyl or methylcyclobutyl moiety is accompanied by a slight decrease in A₁AR binding affinity. The gradual decline in affinity (CPFPX>MCBX>CBX) suggests that the bulkiness of the C8 substituent has considerable influence on receptor-ligand interactions, which is in accordance with the literature [29].

The fundamental suitability of the novel cyclobutyl analogs for imaging the A_1AR was confirmed by *in vitro* autoradiography. Both [^{18}F]CBX and [^{18}F]MCBX showed binding patterns in rat brain that were comparable to [^{18}F]CPFPX binding. The level of non-specific binding was also comparable for all radiotracers, which is consistent with the relatively narrow range of lipophilicity (miLogP between 2.2 and 2.9). These results indicate adequate binding specificity of the novel ligands.

In vivo kinetics of [18 F]CPFPX in rat brain have been evaluated previously [30, 31]. However, additional [18 F]CPFPX reference measurements in rats were conducted in the context of the current study in order to ensure optimal comparability of data. Furthermore, previous [18 F]CPFPX studies in rats conducted by various research groups mainly used reference-tissue based approaches for quantification, therefore available data derived from arterial input functions were limited to the cerebral V_T values reported in [30].

Comparative brain PET studies showed substantial differences in cerebral kinetics of [18 F]CBX, [18 F]MCBX and [18 F]CPFPX in rats. Whole brain SUV curves of [18 F]MCBX peaked much earlier and dropped more steeply than those of [18 F]CPFPX, although peak SUV values of both radiotracers were comparable. Compartmental data analysis indicates that influx and efflux kinetics of [18 F]MCBX are faster compared to [18 F]CPFPX (higher K_1 and k_2 values), but the extent of brain uptake is similar (similar K_1/k_2 and V_T). These results support the assumption that the different shapes of the brain

SUV curves of the two radiotracers are caused by variations in transport kinetics. Most likely, the differences in cerebral kinetics between [18F]MCBX and [18F]CPFPX can be attributed to a combination of the higher peripheral clearance observed with [18F]MCBX [22] and faster drugreceptor binding kinetics as indicated by the lower A₁AR affinity of [¹⁸F]MCBX. Variations in plasma and brain free fractions might be another factor leading to differences in brain exposure and cerebral kinetics. Plasma free fractions of [18F]CPFPX, [18F]MCBX and [18F]CBX in the rat were 1.7%, 4.3% and 2.7% [22]. Since these values are clustered within a relatively narrow range, the influence of this parameter on brain exposure will probably be relatively small. Free fractions in brain are inherently difficult to determine experimentally, therefore plasma free fraction are often used as a surrogate to estimate the effect of brain tissue binding on brain partitioning and receptor-ligand interactions. With regard to the plasma free fractions of the three xanthines, largest physiological differences would be expected between [18F]CPFPX and [18F]MCBX. However, the influence of protein binding on physiological processes such as membrane permeation and thus the validity of the free drug hypothesis [32] has been increasingly questioned in recent years [33], since numerous experimental studies reported apparent discrepancies between predicted and observed physiological properties (e.g., uptake and clearance rates) especially of highly bound drugs [34-38]. It is therefore difficult to give a quantitative estimation of the effects of the 2.5-times higher plasma free fraction of [18F]MCBX on the cerebral characteristics of this radioligand.

A potential benefit of faster radiotracer kinetics in brain is the reduction of the minimum scan time required for quantification of kinetic parameters [39]. Common modeling approaches require the capture of all three kinetic phases of receptor-ligand interactions following bolus injection (uptake, equilibrium and washout phase) to properly derive the receptor parameters [1]. Reasonably short acquisition times are especially relevant in the context of clinical studies, since long PET scan durations decrease economic efficiency and patient compliance, and increase the occurrence of motion artefacts which require extensive correction procedures. The minimal duration of the scan required to achieve time-independent derivation of cerebral V_T was compared between [18 F]CPFPX

and [18 F]MCBX. Considerable shortening of [18 F]CPFPX data sets was possible without resulting in large bias or problems with fit convergence. Despite marked inter-individual differences in brain kinetics, a scan time of about 90 min proved to be sufficient for reliable V_T quantification in all tested animals. With [18 F]MCBX, a lack of convergence was frequently encountered when fitting the 2TCM to the shortened data sets, presumably as a result of the higher influence of noise in later time frames with low cerebral radioactivity concentrations. For two animals, very short scan times of less than 30 min were sufficient for V_T quantification, confirming the assumption that the lower affinity and higher plasma clearance of [18 F]MCBX should result in shorter minimal scan times as compared to [18 F]CPFPX. However, since the data sets of the other two animals could not be analyzed equally well due to problems with fitting convergence, no definitive conclusion on the effect of different kinetic characteristics of the two radiotracers on minimal scan duration can be deduced.

With [18 F]CBX, only a very low degree of brain uptake could be observed (tissue-to-plasma SUV ratio < 1). A closer analysis of the cerebral kinetics of [18 F]CBX suggests that this behavior results from the lower affinity of this analog and, to some extent, its lower lipophilicity. Calculated V_T (which is equivalent to K_1/k_2 in the 1TCM) amounts to only about % of the values obtained for [18 F]CPFPX and [18 F]MCBX, indicating that the retention of the radiotracer in brain is insufficient. Due to the unfavorable signal-to-background ratio encountered in [18 F]CBX imaging data which hampered fitting of the individual rate constants, in-depth analysis of the individual transport processes was not feasible. However, since the differences in lipophilicity between [18 F]CBX on the one hand and [18 F]MCBX and [18 F]CPFPX on the other hand are relatively small, it seems obvious that affinity is the decisive factor determining brain pharmacokinetics of the radiolabeled xanthines. The considerably higher amount of [18 F]CBX available to the brain (higher plasma concentration), could not compensate for the negative effect of its lower binding affinity. Additionally, cerebral characteristics of [18 F]CBX might also be influenced to some extent by efflux transport at the blood brain barrier. Ishiwata at el. reported an increase in uptake and brain-to-blood ratio of the 1,3,8-substituted xanthine [11 C]MPDX after treatment of mice with the P-glycoprotein (P-gp) inhibitor cyclosporine A

[40]. The susceptibility of [18F]CPFPX and its cyclobutyl-substituted analogs to P-gp mediated efflux has not yet been investigated, however, this aspect is surely a worthwhile focus for future research.

The current study demonstrates that the suitability of a candidate radioligand for *in vivo* PET imaging cannot be readily predicted on the basis of isolated characteristics (e.g., lipophilicity, binding affinity, protein binding, metabolic stability) of the novel compound. This is caused by the mutual interdependence of these factors and their combined impact on brain pharmacokinetics. *In vivo* performance of the xanthine A₁AR radioligands was mainly governed by their binding affinity. Variations in plasma concentrations and cerebral kinetics had only a minor impact on PET data quality.

Conclusions

Although [18 F]CBX and [18 F]MCBX do not represent an improvement over [18 F]CPFPX for PET imaging of A $_1$ AR, the results obtained in this study provide valuable information regarding the effects of different physicochemical and pharmacological properties on the cerebral pharmacokinetics of xanthine-derived A $_1$ AR radioligands which can be used to adjust future strategic development processes for novel PET tracers.

Abbreviations

1TCM: One-tissue compartment model; 2TCM: Two-tissue compartment model; A_1AR : A_1 adenosine receptor; CBX: 8-Cyclobutyl-3-(3-fluoropropyl)-1-propylxanthine; CPFPX: 8-Cyclopentyl-3-(3-fluoropropyl)-1-propylxanthine; DPCPX: 8-Cyclopentyl-1,3-dipropylxanthine; GTP: Guanosine-5'-triphosphate; K_d : Dissociation constant; K_i : Inhibition constant; MCBX: 3-(3-Fluoropropyl)-8-(1-methylcyclobutyl)-1-propylxanthine; PET: Positron emission tomography; P-gp: P-Glycoprotein; p.i.: Post injection; ROI: Region of interest; SD: standard deviation; SUV: Standardized uptake value; TAC: Time-activity curve; V_S : Specific distribution volume; V_T : Total distribution volume

References

- [1] Laruelle M, Slifstein M, Huang Y. Relationships between radiotracer properties and image quality in molecular imaging of the brain with positron emission tomography. Mol Imaging Biol 2003;5:363–75.
- [2] Porkka-Heiskanen T. Adenosine in sleep and wakefulness. Ann Med 1999;31:125–9.
- [3] Portas CM, Thakkar M, Rainnie DG, Greene RW, McCarley RW. Role of adenosine in behavioral state modulation: a microdialysis study in the freely moving cat. Neuroscience 1997;79:225–35.
- [4] Kim Y, Elmenhorst D, Weisshaupt A, Wedekind F, Kroll T, McCarley RW, et al. Chronic sleep restriction induces long-lasting changes in adenosine and noradrenaline receptor density in the rat brain. J Sleep Res 2015;24:549–58.
- [5] Mendonça Ad, Ribeiro JA. Adenosine and synaptic plasticity. Drug Dev. Res. 2001;52:283–90.
- [6] Maia L, Mendonca A de. Does caffeine intake protect from Alzheimer's disease? Eur J Neurol 2002;9:377–82.
- [7] Rahman A. The Role of Adenosine in Alzheimers Disease. CN 2009;7:207–16.
- [8] Fuxe K, Strömberg I, Popoli P, Rimondini-Giorgini R, Torvinen M, Ogren SO, et al. Adenosine receptors and Parkinson's disease. Relevance of antagonistic adenosine and dopamine receptor interactions in the striatum. Adv Neurol 2001;86:345–53.
- [9] Cieślak M, Komoszyński M, Wojtczak A. Adenosine A_{2A} receptors in Parkinson's disease treatment. Purinergic Signalling 2008;4:305–12.
- [10] Ferré S. Adenosine-dopamine interactions in the ventral striatum. Implications for the treatment of schizophrenia. Psychopharmacology (Berl.) 1997;133:107–20.
- [11] Ribeiro J, Sebastião A, Mendonça A de. Adenosine receptors in the nervous system: pathophysiological implications. Prog Neurobiol 2003;68:377–92.
- [12] Baraldi PG, Tabrizi MA, Gessi S, Borea PA. Adenosine receptor antagonists: translating medicinal chemistry and pharmacology into clinical utility. Chem Rev 2008;108:238–63.
- [13] Yuzlenko O, Kieć-Kononowicz K. Potent adenosine A₁ and A_{2A} receptors antagonists: recent developments. Curr Med Chem 2006;13:3609–25.

- [14] Holschbach MH, Olsson RA, Bier D, Wutz W, Sihver W, Schüller M, et al. Synthesis and evaluation of no-carrier-added 8-cyclopentyl-3-(3-[18F]fluoropropyl)-1-propylxanthine ([18F]CPFPX): a potent and selective A₁-adenosine receptor antagonist for in vivo imaging. J Med Chem 2002;45:5150–6.
- [15] Bauer A, Holschbach MH, Cremer M, Weber S, Boy C, Shah NJ, et al. Evaluation of 18 F-CPFPX, a novel adenosine A_1 receptor ligand: in vitro autoradiography and high-resolution small animal PET. J Nucl Med 2003;44:1682–9.
- [16] Nabbi-Schroeter D, Elmenhorst D, Oskamp A, Laskowski S, Bauer A, Kroll T. Effects of Long-Term Caffeine Consumption on the Adenosine A₁ Receptor in the Rat Brain: an In Vivo PET Study with [18F]CPFPX. Mol Imaging Biol 2018;20:284–91.
- [17] Elmenhorst E, Elmenhorst D, Benderoth S, Kroll T, Bauer A, Aeschbach D. Cognitive impairments by alcohol and sleep deprivation indicate trait characteristics and a potential role for adenosine A₁ receptors. Proc Natl Acad Sci U S A 2018;115:8009–14.
- [18] Elmenhorst D, Elmenhorst E, Hennecke E, Kroll T, Matusch A, Aeschbach D, et al. Recovery sleep after extended wakefulness restores elevated A₁ adenosine receptor availability in the human brain. Proc Natl Acad Sci U S A 2017;114:4243–8.
- [19] Kreft S, Bier D, Holschbach MH, Schulze A, Coenen HH. New potent A₁ adenosine receptor radioligands for positron emission tomography. Nucl Med Biol 2017;44:69–77.
- [20] Bier D, Holschbach MH, Wutz W, Olsson RA, Coenen HH. Metabolism of the A₁ adenosine receptor positron emission tomography ligand [¹⁸F]8-cyclopentyl-3-(3-fluoropropyl)-1-propylxanthine ([¹⁸F]CPFPX) in rodents and humans. Drug Metab Dispos 2006;34:570–6.
- [21] Matusch A, Meyer PT, Bier D, Holschbach MH, Woitalla D, Elmenhorst D, et al. Metabolism of the A₁ adenosine receptor PET ligand [¹⁸F]CPFPX by CYP1A2: implications for bolus/infusion PET studies. Nucl Med Biol 2006;33:891–8.

- [22] Schneider D, Oskamp A, Holschbach M, Neumaier B, Bauer A, Bier D. Relevance of In Vitro Metabolism Models to PET Radiotracer Development: Prediction of In Vivo Clearance in Rats from Microsomal Stability Data. Pharmaceuticals (Basel) 2019;12.
- [23] Schneider D, Bier D, Bauer A, Neumaier B, Holschbach M. Influence of incubation conditions on microsomal metabolism of xanthine-derived A₁ adenosine receptor ligands. J Pharmacol Toxicol Methods 2019;95:16–26.
- [24] Lohse MJ, Klotz KN, Jakobs KH, Schwabe U. Barbiturates are selective antagonists at A₁ adenosine receptors. J Neurochem 1985;45:1761-70.
- [25] Neuhoff V, Philipp K, Zimmer HG, Mesecke S. A simple, versatile, sensitive and volume-independent method for quantitative protein determination which is independent of other external influences. Hoppe-Seyler's Z Physiol Chem 1979;360:1657–70.
- [26] Katz JJ, Todd MM, Warner DS. Quantitative comparison of cerebral blood volume in rats receiving halothane or isoflurane. Anesthesiology 1988;69:A534.
- [27] Fastbom J, Pazos A, Palacios J. The distribution of adenosine A_1 receptors and 5'-nucleotidase in the brain of some commonly used experimental animals. Neuroscience 1987;22:813–26.
- [28] Weber RG, Jones CR, Lohse MJ, Palacios JM. Autoradiographic Visualization of A₁ Adenosine Receptors in Rat Brain with [³H]8-Cyclopentyl-1,3-Dipropylxanthine. J Neurochem 1990;54:1344–53.
- [29] Müller CE, Jacobson KA. Xanthines as Adenosine Receptor Antagonists. In: Fredholm BB, editor.

 Methylxanthines. Berlin, Heidelberg: Springer Berlin Heidelberg; 2011, p. 151–99.
- [30] Elmenhorst D, Kroll T, Wedekind F, Weisshaupt A, Beer S, Bauer A. In Vivo Kinetic and Steady-State Quantification of ¹⁸F-CPFPX Binding to Rat Cerebral A₁ Adenosine Receptors: Validation by Displacement and Autoradiographic Experiments. J Nucl Med 2013;54:1411–9.
- [31] Kroll T, Elmenhorst D, Weisshaupt A, Beer S, Bauer A. Reproducibility of Non-Invasive A₁

 Adenosine Receptor Quantification in the Rat Brain Using [¹⁸F]CPFPX and Positron Emission

 Tomography. Mol Imaging Biol 2014;16:699–709.

- [32] Liu X, Chen C. Free Drug Hypothesis for CNS Drug Candidates. In: Di L, Kerns EH, editors. Blood-Brain Barrier in Drug Discovery. Hoboken, NJ: John Wiley & Sons, Inc; 2015, p. 42–65.
- [33] Smith DA, Di L, Kerns EH. The effect of plasma protein binding on in vivo efficacy: misconceptions in drug discovery. Nat Rev Drug Discov 2010;9:929–39.
- [34] Poulin P, Burczynski FJ, Haddad S. The Role of Extracellular Binding Proteins in the Cellular Uptake of Drugs: Impact on Quantitative In Vitro-to-In Vivo Extrapolations of Toxicity and Efficacy in Physiologically Based Pharmacokinetic-Pharmacodynamic Research. J Pharm Sci 2016;105:497–508.
- [35] Poulin P, Haddad S. Albumin and Uptake of Drugs in Cells: Additional Validation Exercises of a Recently Published Equation that Quantifies the Albumin-Facilitated Uptake Mechanism(s) in Physiologically Based Pharmacokinetic and Pharmacodynamic Modeling Research. J Pharm Sci 2015;104:4448–58.
- [36] Baker M, Parton T. Kinetic determinants of hepatic clearance: Plasma protein binding and hepatic uptake. Xenobiotica. 2007;37:1110–34.
- [37] Pardridge WM. Targeted Delivery of Hormones to Tissues by Plasma Proteins. In: Terjung R, editor. Comprehensive Physiology. Hoboken, NJ, USA: John Wiley & Sons, Inc; 2010, p. 335–82.
- [38] Jones DR, Hall SD, Jackson EK, Branch RA, Wilkinson GR. Brain uptake of benzodiazepines: effects of lipophilicity and plasma protein binding. J Pharmacol Exp Ther 1988;245:816–22.
- [39] Huang Y, Hwang D, Narendran R, Sudo Y, Chatterjee R, Bae S, et al. Comparative Evaluation in Nonhuman Primates of Five PET Radiotracers for Imaging the Serotonin Transporters: [11C]McN 5652, [11C]ADAM, [11C]DASB, [11C]DAPA, and [11C]AFM. J Cereb Blood Flow Metab 2002;22:1377–98.
- [40] Ishiwata K, Kawamura K, Yanai K, Hendrikse NH. In Vivo Evaluation of P-Glycoprotein Modulation of 8 PET Radioligands Used Clinically. J Nucl Med 2007;48:81-87.

Tables

Table 1. Injected radioactivity, mass and amount of radiotracer. Mean values (SD), n=4

Radiotracer	Injected radioactivity / MBq	Injected amount of radiotracer / nmol	Injected mass of radiotracer / μg
[¹⁸ F]CBX	21.4 (2.8)	0.50 (0.21)	0.15 (0.06)
[¹⁸ F]MCBX	21.7 (1.3)	0.39 (0.31)	0.13 (0.10)
[¹⁸ F]CPFPX	21.8 (1.4)	0.41 (0.07)	0.13 (0.02)

Table 2. Measured A₁AR affinities of the xanthine compounds. Mean values (SD).

Ligand	Number of experiments	K _i / nM
СВХ	4	10.0 (0.52)
MCBX	3	3.3 (0.30)
СРГРХ	3	1.4 (0.15)

Table 3. Results of graphical analysis and compartmental modeling of cerebral PET data (whole brain ROI). K_1 and k_2 were derived either from 1TCM fits ([18 F]CBX) or 2TCM fits ([18 F]MCBX, [18 F]CPFPX).

Kinetic parameter	Model	[¹⁸ F]CBX	[¹⁸ F]MCBX	[¹⁸ F]CPFPX
V _T / ml/cm ³	LGA	0.641 (0.184) ^{bc}	2.648 (0.717) ^a	2.678 (0.980) ^a
V _T / ml/cm ³	1TCM/2TCM	0.620 (0.192) ^{bc}	2.716 (0.791) ^a	2.703 (1.015) ^a
V _s / ml/cm ³	2TCM	n.d.	0.496 (0.205)	0.653 (0.262)
K ₁ / ml/cm ³ /min	1TCM/2TCM	0.124 (0.039) ^b	0.366 (0.097) ^{ac}	0.172 (0.059) ^b
k ₂ / min ⁻¹	1TCM/2TCM	0.202 (0.022)	0.170 (0.040)	0.093 (0.037)
k ₃ / min ⁻¹	2TCM	n.d.	0.027 (0.044)	0.025 (0.039)
k ₄ / min ⁻¹	2TCM	n.d.	0.075 (0.093)	0.039 (0.030)
K ₁ /k ₂ / ml/cm ³	1TCM/2TCM	0.620 (0.192)*	2.219 (0.740)	2.049 (0.998)
k ₃ /k ₄ / 1/1	2TCM	n.d.	0.239 (0.136)	0.418 (0.383)

LGA, Logan graphical analysis; 1TCM, one-tissue compartment model; 2TCM, two-tissue compartment model; V_T , total distribution volume; V_S , specific distribution volume; K_1 - k_4 , transfer rate constants; n.d., not determined; * K_1 / k_2 equals V_T in 1TCM; ^a significantly different from [¹⁸F]CBX; ^b significantly different from [¹⁸F]CPFPX (p<0.05, one-way ANOVA with post-hoc Tukey test or independent t-test if appropriate). Mean values (SD), n = 4.

Figure Legends

Figure 1. Chemical structures of [¹⁸F]CPFPX, [¹⁸F]MCBX, [¹⁸F]CBX and their ¹⁸F-isotopologues. The varying substituents at the xanthine C8 position are highlighted in blue [22]. miLogP values were calculated using the Molinspiration milogP2.2 algorithm.

Figure 2. Representative autoradiographs of sagittal rat brain slices after incubation with 0.4-0.5 nM [18 F]CBX (a, b), [18 F]MCBX (c, d) and [18 F]CPFPX (e, f). Figures on the left side show total binding of the radiotracer, figures on the right side show non-specific binding in the presence of 13 μ M DPCPX. High accumulation of radioactivity (warm colours) were found in hippocampus (hip), thalamus (th), cerebellar cortex (cbl) and neocortex (ctx).

Figure 3. Representative PET images of rat brain after i.v. bolus administration of 20-22 MBq [¹⁸F]CBX (a, b), [¹⁸F]MCBX (c, d) and [¹⁸F]CPFPX (e, f). 180-min scans were conducted under isoflurane anesthesia. Activity concentration values registered 0-60 min p.i. were averaged (time-weighted average) and normalized to body weight and amount of injected radioactivity. SUV maximum was set to 5 g/ml (left side: sagittal plane, right side: horizontal plane; cbl, cerebellum; ctx, neocortex; hip, hippocampus; hg, Harderian glands; th, thalamus).

Figure 4. Kinetics of [¹⁸F]CBX (a), [¹⁸F]MCBX (b) and [¹⁸F]CPFPX (c) in whole rat brain (black squares) and arterial plasma (red circles) following single bolus injection of 20-22 MBq radiotracer. 180-min scans were conducted under isoflurane anesthesia. SUVs were calculated by normalizing radioactivity concentration to amount of injected radioactivity and body weight. Plasma data were corrected for metabolites. Solid lines are a guide to the eye. Data (mean values ± SD) were obtained from 4 animals per radiotracer.

Figure 5. Representative 2TCM fits (left row) and Logan plots (right row) of brain activity data acquired after i.v. bolus injection of 21-22 MBq [18 F]CBX (a, b), [18 F]MCBX (c, d) and [18 F]CPFPX (e, f). 180-min scans were conducted under isoflurane anesthesia. Black symbols represent measured data, red solid lines represent model fits (C_P , plasma time-activity curve; C_T , tissue time-activity curve).

Figures

Fig. 1

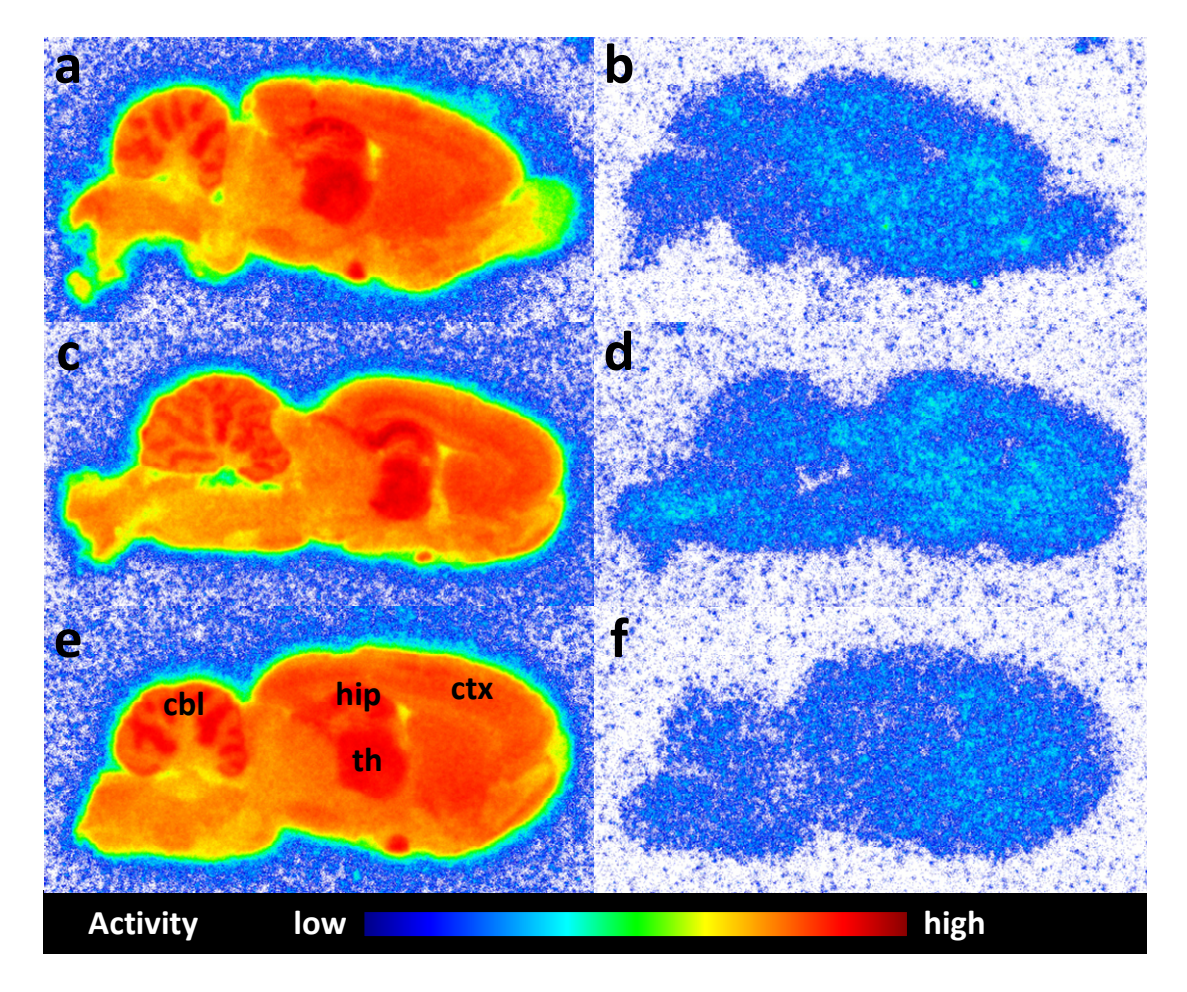


Fig. 2

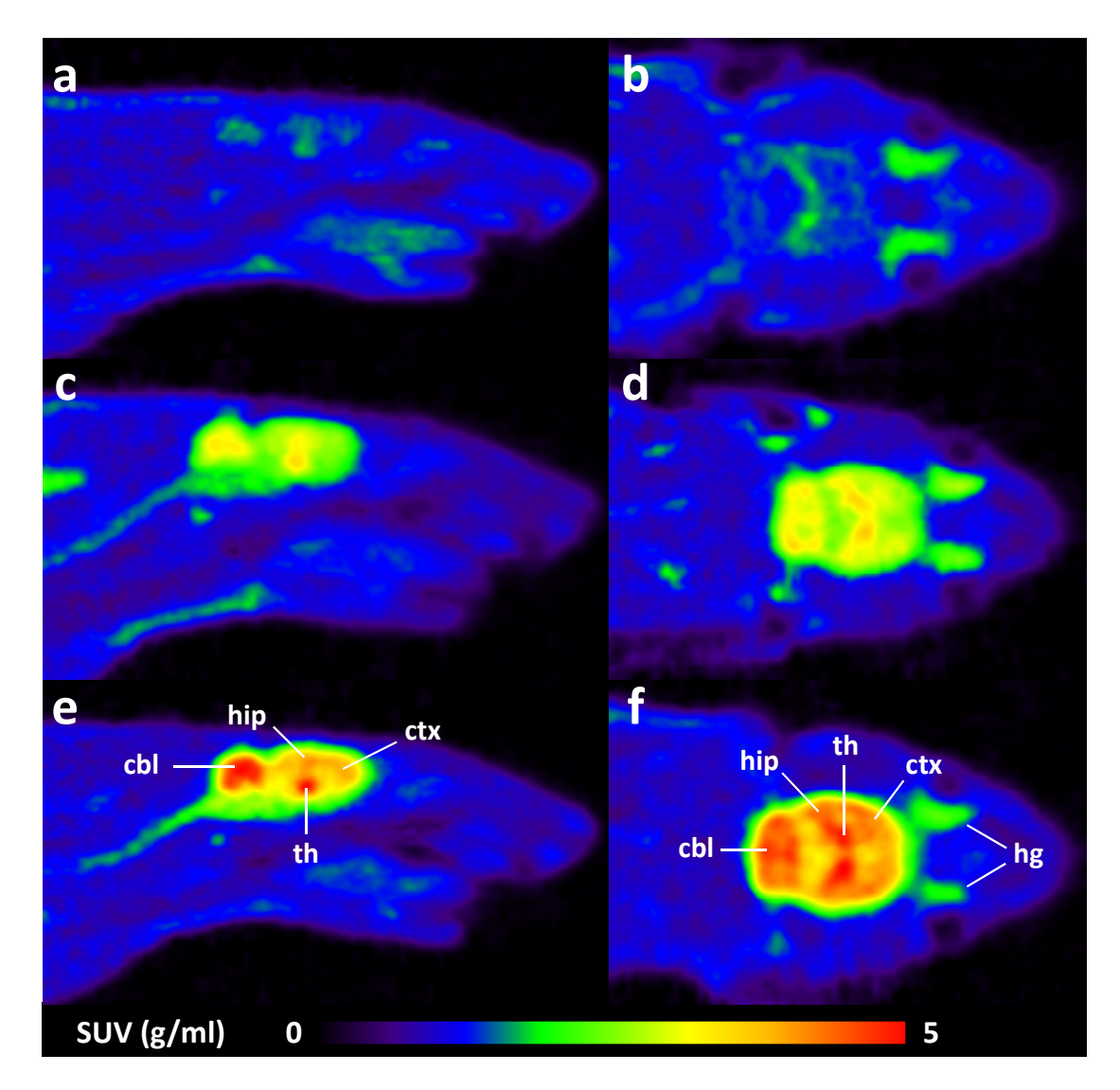


Fig. 3

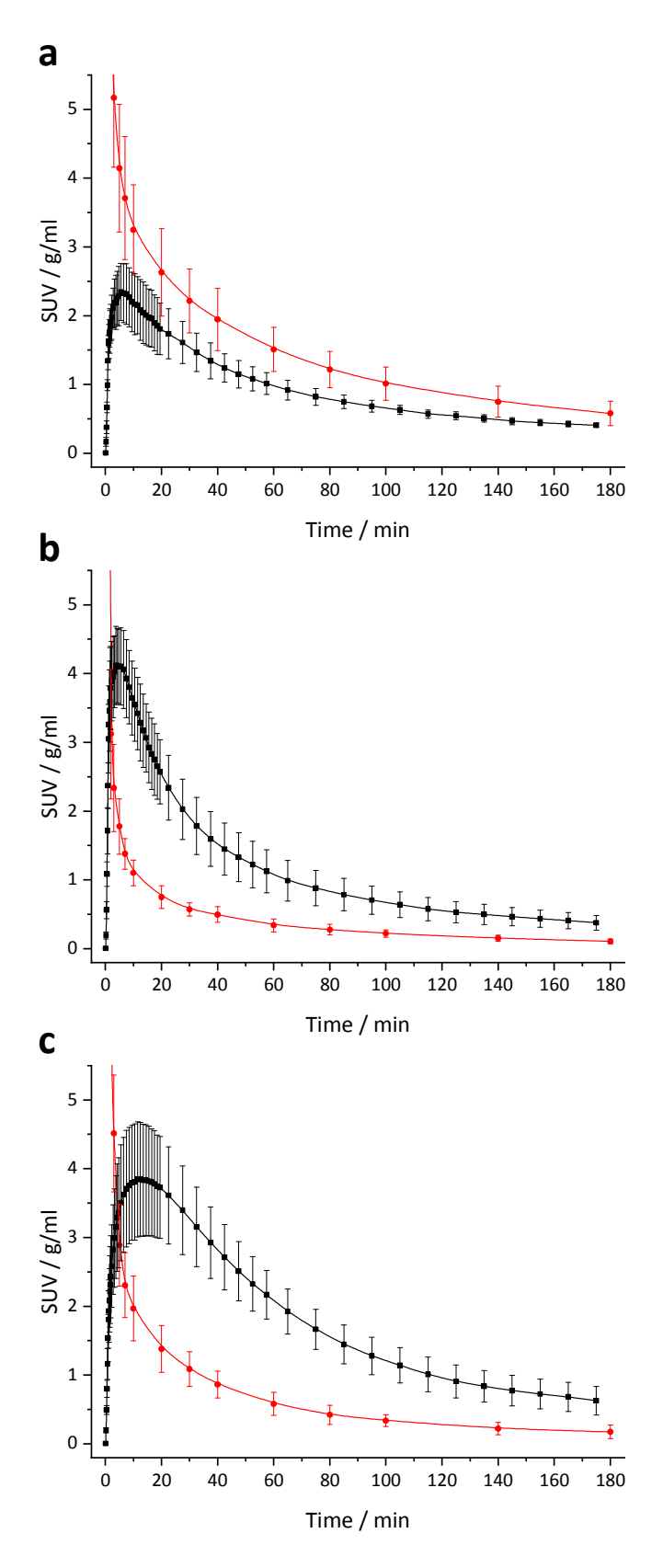


Fig. 4

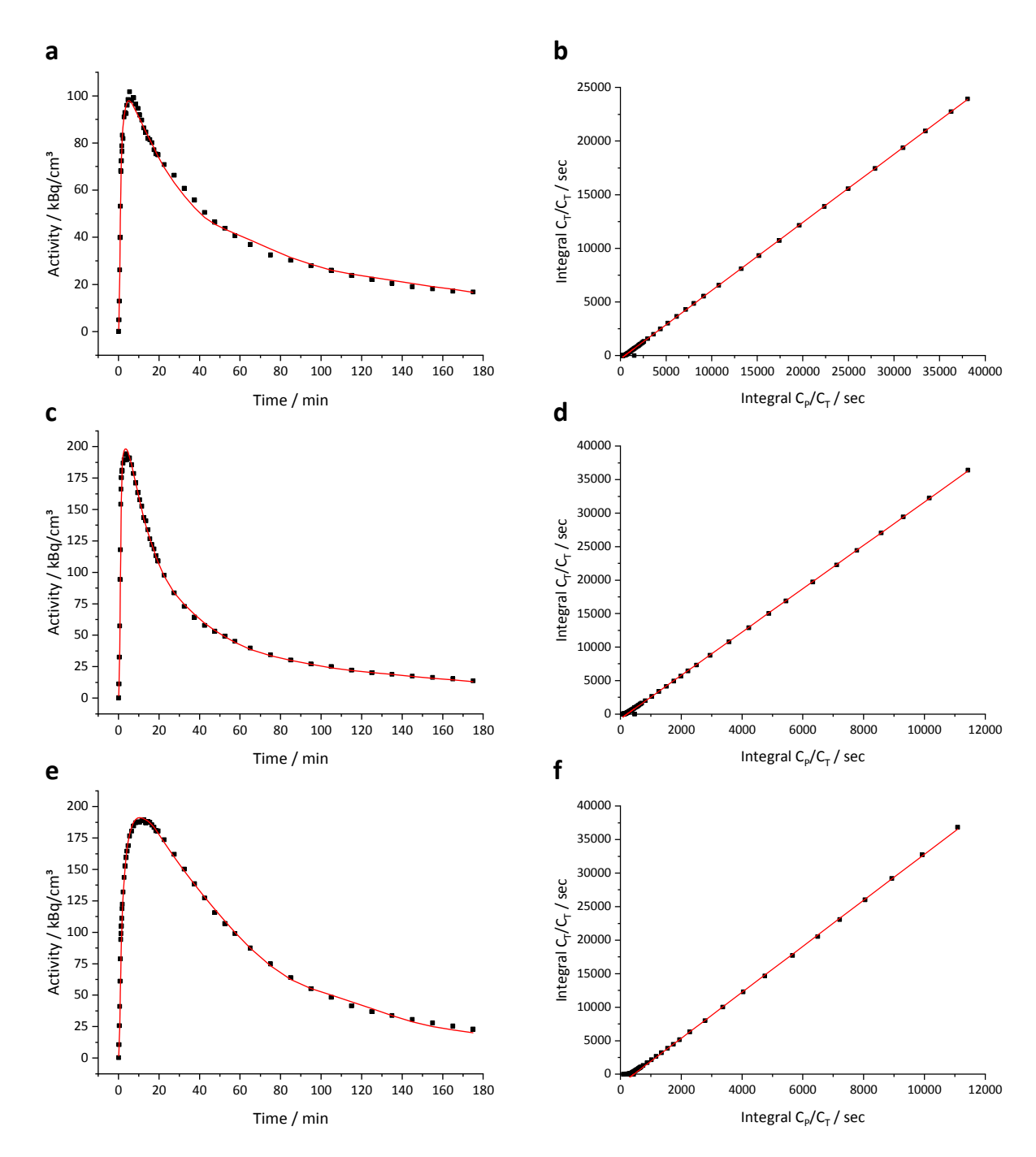


Fig. 5